

GEV γ -RAY EMISSION FROM M33 AND ARP 299SHAO-QIANG XI^{1,2}, HAI-MING ZHANG^{1,2}, RUO-YU LIU^{1,2}, XIANG-YU WANG^{1,2}¹School of Astronomy and Space Science, Nanjing University, Nanjing 210023, China; xywang@nju.edu.cn²Key laboratory of Modern Astronomy and Astrophysics (Nanjing University), Ministry of Education, Nanjing 210023, China

ABSTRACT

Star-forming galaxies are huge reservoirs of cosmic rays (CRs) and these CRs convert a significant fraction of their energy into γ -rays by colliding with the interstellar medium (ISM). Several nearby star-forming galaxies have been detected in GeV-TeV γ -rays. It is also found that the γ -ray luminosities in 0.1-100 GeV correlate well with indicators of star formation rates of the galaxies, such as the total infrared (IR) luminosity. In this paper, we report a systematic search for possible γ -ray emission from galaxies in the IRAS Revised Bright Galaxies Sample, using 11.4 years of γ -ray data taken by the *Fermi* Large Area Telescope (LAT). Two new galaxies, M33 and Arp 299, are detected significantly. The two galaxies are consistent with the empirical correlation between the γ -ray luminosity and total infrared luminosity, suggesting that their γ -ray emissions should mainly originate from CRs interacting with ISM. Nevertheless, there is a tentative evidence that the flux of the γ -ray emission from Arp 299 is variable. If the variability is true, part of the emission from Arp 299 should originate from the obscured AGN in this interacting galaxy system. In addition, we find that the γ -ray excess from M33 is located at the northeast region of the galaxy, where a supergiant H II region, NGC604, resides. This indicates that some bright star-forming regions in spiral galaxies could play a dominant role in the galaxy in producing γ -ray emission.

1. INTRODUCTION

It is believed that Galactic cosmic rays (CRs) are accelerated by supernova remnant (SNRs) or massive star clusters in our Galaxy. CR protons interact with the interstellar gas and produce neutral pions (schematically written as $p+p \rightarrow \pi^0 + \text{other products}$), which in turn decay into γ -rays ($\pi^0 \rightarrow \gamma + \gamma$). Seven star-forming galaxies have been firmly detected in γ -rays with the Fermi Large Area Telescope (LAT), including the Large Magellanic Cloud (LMC; [Abdo et al. 2010d](#); [Ackermann et al. 2016](#)), the Small Magellanic Cloud ([Abdo et al. 2010b](#)), the Andromeda galaxy M31 ([Abdo et al. 2010c](#)), starburst galaxies M82 and NGC 253 ([Abdo et al. 2010a](#)), NGC 2146 ([Tang et al. 2014](#)) and Arp 220 ([Peng et al. 2016](#); [Griffin et al. 2016](#)). In addition, a few star-forming galaxies with obscured active galactic nuclei (AGNs), such as NGC 1068, NGC 4945, NGC 3424 and UGC 11041, have been detected by *Fermi*-LAT ([Ackermann et al. 2012](#); [Peng et al. 2019](#)).

Noting the connection between star formations and CRs in starburst galaxies, some authors have proposed scaling relationships between star formation rates (SFRs) and γ -ray luminosities ([Pavlidou & Fields 2002](#); [Torres 2004](#); [Thompson et al. 2007](#); [Stecker 2007](#); [Persic & Rephaeli 2010](#); [Lacki et al. 2011](#)). SFR indicators include the total infrared (IR) luminosity in 8 – 1000 μm

([Kennicutt 1998](#)), and radio continuum luminosity at 1.4 GHz produced by synchrotron emitting CR electrons ([Yun et al. 2001](#)). With the accumulation of *Fermi*-LAT data, the correlation between γ -ray luminosities and SFR indicators are first found in [Abdo et al. \(2010c\)](#). [Ackermann et al. \(2012\)](#) studied a sample of 69 dwarf, spiral, and luminous and ultraluminous IR galaxies using 3 years of data collected by *Fermi*-LAT. They find further evidence for quasi-linear scaling relation between the γ -ray luminosity and total infrared luminosity. This correlation was later extended to higher luminosity galaxies with γ -ray detection from a luminous IR galaxy, NGC 2146 ([Tang et al. 2014](#)), and an ultraluminous IR galaxy, Arp 220 ([Peng et al. 2016](#); [Griffin et al. 2016](#)).

In this paper, we report a systematic search for possible γ -ray emission from galaxies in the IRAS Revised Bright Galaxies Sample, using 11.4 years of γ -ray data collected by the *Fermi*-LAT telescope. While the result of detection of GeV emission from M33 and Arp 299 has been briefly mentioned in our previous paper ([Xi et al. 2020](#), hereafter Paper I), here we present the details of the two γ -ray sources and discuss the nature of their emissions. The paper is organized as follows. In §2, we present a description of the galaxy sample selection and the *Fermi*-LAT data analysis procedure. In §3, we

present the results of the analysis. In §4, we discuss the nature of the γ -ray emissions from M33 and Arp 299.

2. DATA SET AND ANALYSIS METHODS

The scaling relation reported in [Ackermann et al. \(2012\)](#) implies the γ -ray detection is likely associated with bright IR galaxies. We selected our sample galaxies from the IRAS Revised Bright Galaxies Sample¹ ([Sanders et al. 2003](#)), excluding the 15 IR-bright galaxies that have been detected in γ -rays with *Fermi*-LAT and listed in *Fermi*-LAT Fourth Source Catalog (4FGL; [Abdollahi et al. 2020](#)). We performed the standard sequence of analysis steps for each galaxies (described in our Paper I), resulting in the detection of two new γ -ray sources that are, respectively, spatially coincident with M33 and Arp 299. The details of the analysis for these two galaxies are given as below.

Fermi-LAT is a pair-conversion telescope covering the energy range from 20 MeV to more than 300 GeV with a field of view of 2.4 sr ([Atwood et al. 2009](#)). For the analysis in this work, we employed recent developments of the Science Tools and use the *Fermi*-LAT Pass 8 Source class events collected in ~ 11.4 yr, which include both front and back-converted LAT events and correspond to P8R3_SOURCE_V2 instrument response functions, but exclude the events with a zenith angle larger than 90° in order to remove the contaminant from the Earth limb.

For the galaxy M33, we selected the events in the energy range 0.3 – 500 GeV and within a rectangular **region of interest** (ROI) of size $17^\circ \times 17^\circ$ centered at M33 IR center ($\alpha_{2000} = 23.475^\circ, \delta_{2000} = 30.669^\circ$). We used *gtmktime* tool to select time intervals expressed by (DATA_QUAL > 0) && (LAT_CONFIG == 1), and binned the data in 20 logarithmically spaced bins in energy and in a spatial bin of 0.025° per pixel. The γ -ray background model consists of the latest template *gll_iem_v7.fits* for Galactic interstellar emission and the isotropic template with a spectrum described by the file *iso_P8R3_SOURCE_V2_v01.txt*, as well as the sources listed in the 4FGL catalog within 20° around M33. One possible shortcoming of using the 4FGL catalog (based on 8 years of LAT observations) to perform the search within a data set covering 11.4 yr is that unrelated new point sources may be discovered inside the ROI of the target source, which may influence the analysis. We produce a $6^\circ \times 6^\circ$ map of the Test Statistic (TS)² centered

at M33 **IR** center to search for the new background γ -ray sources.³ The criteria of the new **background** source is that the γ -ray excess has a significance of $TS > 25$ above the diffuse background and has an angular separation larger than 0.3° from the center of M33. We find three new background sources and include them in our background model for M33 (see the appendix A).

For the galaxy Arp 299, we selected the events in the energy range 0.3 – 500 GeV within a rectangular ROI of size $17^\circ \times 17^\circ$ centered at the galaxy IR center ($\alpha_{2000} = 172.136^\circ, \delta_{2000} = 58.561^\circ$). The rest steps, i.e., the data filter, data bin and background modeling are carried out with similar approaches to what have been done for M33. There is a new background source in the $6^\circ \times 6^\circ$ region centered at Arp 299.

In the likelihood analysis, we allow each source within 6.5° from the ROI center to have a free normalization (the 68% containment radius of photons at normal incidence with an energy of 300 MeV is roughly 2.5°). This choice ensures that 99.9% of the predicted γ -ray counts is contained within the chosen radius. The normalizations of the Galactic and isotropic diffuse components are always left free. For the background-only fitting of M33 and Arp 299, we first free the spectral parameter (including normalization and index) of sources within 6.5° region around the galaxies and then fixed the index for subsequent analysis.

3. DATA ANALYSIS RESULTS

3.1. M33

3.1.1. Morphological analysis

[Fig. 1](#) shows the $0.6^\circ \times 0.6^\circ$ TS map in 0.3 – 500 GeV around M33. We find that the position of the TS peak locates at the northeast part of the galaxy. We tested various spatial models and investigated which model is better by employing $\Delta TS = TS_1 - TS_2$, where TS_1 and TS_2 are respectively the TS value of model 1 and model 2 respectively⁴. We first explored the point source models at this best-fit location (i.e., the position of the peak TS value) and at the center of M33, respectively.

³ For the new γ -ray point source, the best location and uncertainty can be determined by maximizing the likelihood value with respect to its position only and using the distribution of Localization Test Statistic (LTS), defined by twice the logarithm of the likelihood ratio of any position with respect to the maximum. Using the $6^\circ \times 6^\circ$ TS map with the resolution of 0.05° per pixel, we determined the position of the new sources at the pixels of the local peak TS value preliminarily. For each new sources, we produced the $0.6^\circ \times 0.6^\circ$ TS and LTS map with the resolution of 0.01° per pixel around the preliminary position to determine the best-fit location and uncertainty, respectively

⁴ Considering the difference in degree of freedom of the model 1 and model 2 is ΔN_{dof} , we can expect the cumulative density of ΔTS follows a χ^2 distribution with ΔN_{dof} degree of freedom. In the case of the same number of degrees of freedom, we simply assume the χ^2 distribution with one degree of freedom.

¹ This is a complete flux-limited sample of all extragalactic objects brighter than 5.24 Jy at $60 \mu m$, covering the entire sky surveyed by IRAS at Galactic latitudes $|b| > 5^\circ$.

² TS is defined as $TS = -2(\ln L_0 - \ln L)$, where L_0 is the maximum-likelihood value for null hypothesis and L is the maximum-likelihood with the additional point source with a power-law spectrum.

Table 1. Spatial template analysis and spectral results of M 33 and Arp 299

Spatial model	TS	<i>R.A.</i>	(Decl.)	$F_{0.1-100\text{GeV}}$	Γ	N_{dof}
(1)	(2)	[deg]	[deg]	[$10^{-12} \text{ erg cm}^{-2} \text{ s}^{-1}$]	(6)	(7)
M33						
Point source (free) ^a	25.1	23.609	30.784	1.28±0.42	2.23±0.24	4
Point source (fixed) ^b	16.7	23.475	30.669	1.34±0.47	2.41±0.26	2
0.23° Disk ^c	23.2	23.475	30.669	1.55±0.35	2.22±0.42	3
Herschel/PACS map (160 μm)	22.8			1.48±0.40	2.22±0.42	2
IRAS map (60 μm)	23.9			1.52±0.40	2.20±0.43	2
Arp 299						
Point source (free) ^a	27.8	172.050	58.526	1.08±0.28	2.07±0.20	4

^a The point source is at the best-fit location. The best-fit location is determined at the position of the peak TS value using the TS map with the resolution of 0.01° per pixel.

^b The point source is at the **IR** center of the **galaxy M33**.

^c The center of the disk model are fixed to the IR center of the **galaxy M33**.

NOTE—(1) Spatial model name; (2) TS value for each spatial model; (3) right ascension J2000; (4) declination J2000; (5) 100 MeV–100 GeV γ –ray average flux; (6) power-law spectral photon index derived by broad band spectrum fitting; (7) degree of freedom for each spatial model .

The TS values are, respectively, 25.1 and 16.7, which suggests that the source is likely to be offset from the galaxy center with a significance 2.4σ . In addition, we considered spatially extended templates based on Herschel/PACS map at $160 \mu\text{m}$ and IRAS map at $60 \mu\text{m}$. These templates are used to test the spatial correlation of the γ -ray emission with star formation sites. The Herschel/PACS and IRAS map models provide better fits ($\sim 2.5\sigma$) to the data than the point source model at the center of M33, but give almost equally good fits as the point source model at the best-fit location. We also test the uniform-brightness disk model with free radius centered at the optical center of M33. The TS value peaks when the radius is 0.23° . We do not find any improvement over the point source model at the best-fit location. The results for all the considered morphological tests are shown in Table 1.

3.1.2. Flux variability

We retained the point source γ model at the best-fit location for examining the variability of the γ -ray flux. We computed light curves in four and eight time bins over 11.4 yr, for events in the energy range 0.3–500 GeV. For the analysis in each time bin, all sources within 6.5° region around M33 have their spectra fixed to the shapes obtained from the above broad band analysis. The result is shown in Figure 2. We then used a likelihood-

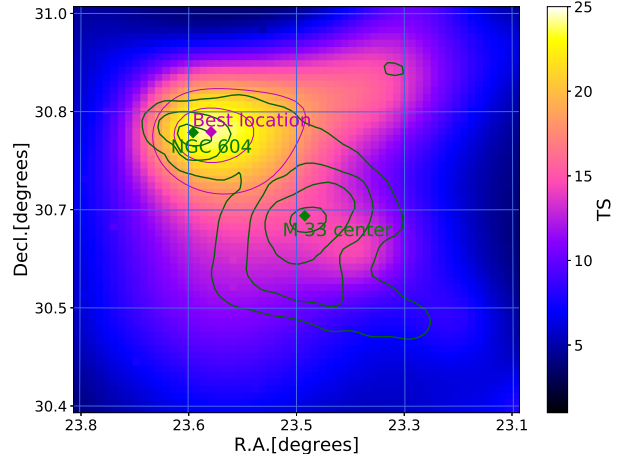


Figure 1. TS map in the energy band 0.3–500 GeV around M33. The purple contours correspond to 68% and 95% confidence region assuming a template of a point-like source at the best-fit location. The dark green contours correspond to the map of IR flux measured by IRAS at $60 \mu\text{m}$.

based statistic to test the significance of the variability. Following the definition in 2FGL (Nolan et al. 2012), the variability index from the likelihood analysis is constructed, with a value in the null hypothesis where the source flux is constant across the full time period, and the value under the alternate hypothesis where the flux in each bin is optimized: $TS_{var} =$

$\sum_{i=1}^N 2 \times (\text{Log}(L_i(F_i)) - \text{Log}(L_i(F_{mean})))$, where L_i is the likelihood corresponding to bin i , F_i is the best-fit flux for bin i , and F_{mean} is the best-fit flux for the full time assuming a constant flux. We get $1.3 - 1.6\sigma$ significance for the flux variability for the analyses using the above two time bins, which suggests no significant variability for the γ -ray emission from M33.

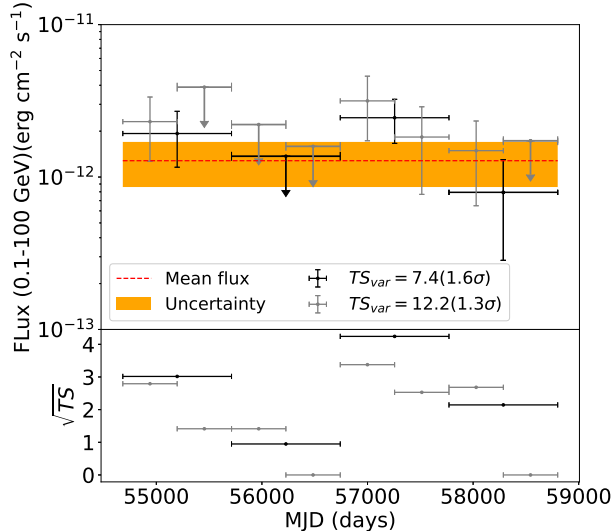


Figure 2. Light curves of M33 with 4 and 8 time bins. The mean flux is the averaged flux over the ~ 11.4 year analysis. The upper limits at 95% confidence level are derived when the TS value for the data points is lower than 4.

3.1.3. Spectral Analysis

For the spectral analysis of M33, we performed a binned maximum likelihood fitting in the $0.3 - 500$ GeV energy range with 20 logarithmic energy bins in total. The power law indices are consistent with each other for the four spatial models, as shown in Table 1. We generated the spectral points based on a maximum likelihood analysis with 4 logarithmic energy bins over $0.3 - 500$ GeV. Within each bin, we used the point source model at the best-fit location and the power law spectrum with a fixed photon index of $\Gamma = 2$ and a free normalization. For the background diffuse components and sources within 6.5° of M33, we fixed their spectral indices to the best-fit values obtained from the above background fitting, but allowing the normalization to vary. We also obtain the spectral point at the energy band $0.1 - 0.3$ GeV to check whether the power-law model is good. We find that the best-fit wide-band power-law model is consistent with all the spectral points, as shown in Fig 3.

3.2. Arp 299

3.2.1. Morphological analysis

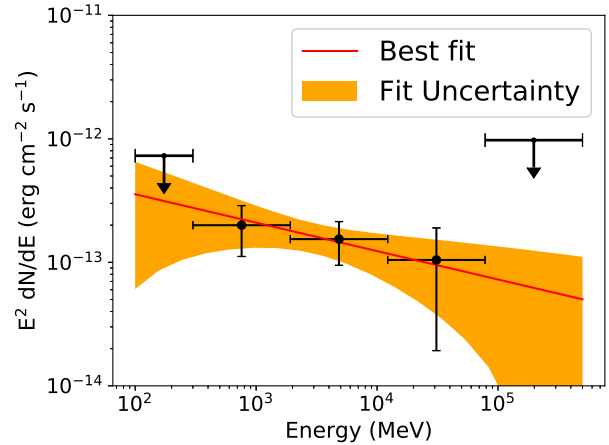


Figure 3. SED for M33 in the energy band $0.1-500$ GeV. The red line and yellow band represent the wide-band best-fit power-law spectrum and the uncertainty **obtained in the energy band $0.3-500$ GeV**. The upper limits at 95% confidence level are derived when the TS value for the data point is lower than 4 ($< 2\sigma$).

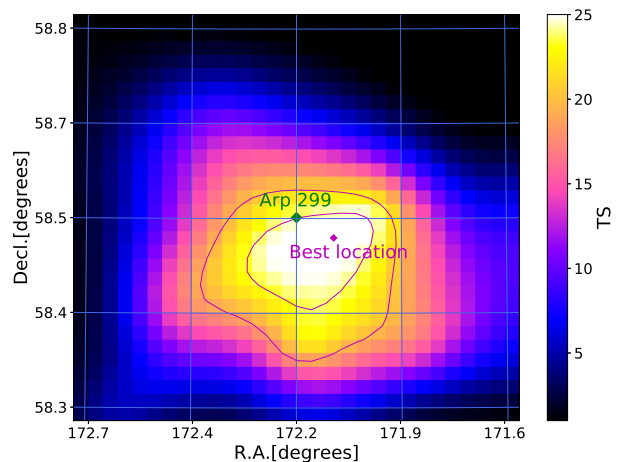


Figure 4. TS map in the energy band $0.3 - 500$ GeV for Arp 299. The purple contours correspond to 68% and 95% confidence region assuming the point-like source template. The dark green diamond correspond to the optical localization of Arp 299.)

Fig. 4 shows the TS map in the $0.3 - 500$ GeV energy range around the galaxy Arp 299. We find that the galaxy position is located within the 68% confidence region of the γ -ray excess.

3.2.2. Flux variability

To examine the variability of the γ -ray flux from Arp 299, we computed light curves in four and eight time bins over 11.4 yr for events in the energy range $0.3 - 500$ GeV. We followed a procedure similar to that used for M33 in Section 3.1.2, and the result is shown in Figure 5. We obtain a variability significance of $2.6 - 2.9\sigma$ for the analyses using the above two time bins, which suggests a mildly significant variability in

the γ -ray emission of Arp 299. We also checked the flux variability with 16 and 40 time bins. We get 3.0σ significance for the flux variability using the 16 time bins, which agrees with the analysis using four and eight time bins. For the 40 time-bin case, we get 0.7σ significance for the flux variability, which seems to indicate less variability on such short timescales. However, we note that, for such a weak γ -ray source, the statistics in each bin in the 40 time-bin analysis may be too low for a reliable analysis.

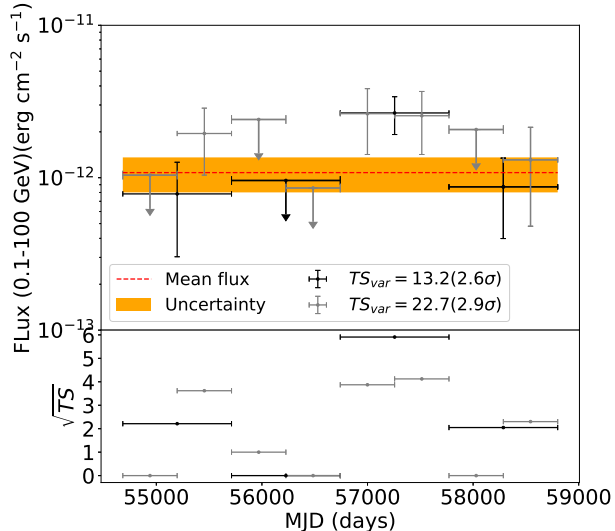


Figure 5. Light curves of Arp 299 with 4 and 8 time bins. The mean flux is the averaged flux over the ~ 11.4 year analysis. The upper limits at 95% confidence level are derived when the TS value for the data points is lower than 4.

3.2.3. Spectral Analysis

For the spectral analysis of Arp 299, we performed a binned maximum likelihood fitting in the 0.3 – 500 GeV energy range with 20 logarithmic energy bins in total considering the point source model. The result is shown in Table. 1. We also generated the spectral points determined by performing a maximum likelihood analysis **in five energy bins** over 0.1 – 500 GeV similar to the case of M33 in Section 3.1.3. As shown in Figure 6, the wide-band power-law model is consistent with these spectral points.

3.3. Non-detected IR galaxies

We derived the 95% C.L. upper limits (UL) for each non-detected galaxy (i.e., $TS < 25$) using the Bayesian method assuming a power-law spectrum with a fixed photon index of 2.2. For NGC 2403, we attribute the γ -ray emission, which is present only in the first 5.7-year *Fermi*-LAT observation (4 Aug. 2014-25 Mar. 2014), to SN 2004dj (see Paper I). Using the last 5.7-year *Fermi*-LAT data (25 Mar. 2014 - 14 Nov. 2019), we derived an

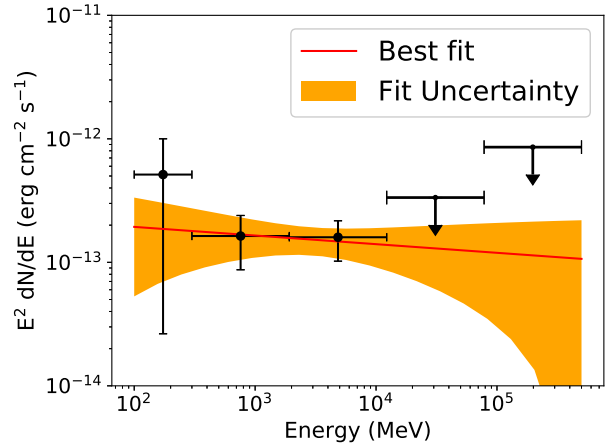


Figure 6. SED for Arp 299 in the energy band 0.1-500 GeV. The red line and yellow band represent the wide-band best-fit power-law spectrum and the uncertainty **obtained in the energy band 0.3-500 GeV**. The upper limits at 95% confidence level are derived when the TS value for the data point is lower than 4.

upper limit for NGC 2403 assuming a point source model at the galaxy center. We compare the ULs on the γ -ray luminosities (0.1 – 100 GeV) to the total IR luminosities (8 – 1000 μ m) for these non-detected IR galaxies, which is shown in Fig 7. We find these non-detected IR galaxies are basically consistent with the empirical $L_\gamma - L_{IR}$ correlation.

4. DISCUSSIONS AND CONCLUSIONS

4.1. M33

As the third largest galaxy in our Local Group, M33 has been considered to be a promising γ -ray source due to its proximity and relatively high gas masses and star formation activity. By using nearly 2 years of *Fermi*-LAT data, [Abdo et al. \(2010c\)](#) searched for the γ -ray emission from M33, but no significant γ -ray emission was detected. [Ackermann et al. \(2017\)](#) revisited the γ -ray emission in the direction M33 using more than 7 yr of LAT Pass 8 data in the energy range 0.1 – 100 GeV, but still found no significant detection. More recently, [Karwin et al. \(2019\)](#) found positive residual towards the M33 region. Di Mauro et al. (2019) reported M33 as a point-like source with $TS = 39.4$ in the energy band 0.3 – 1000 GeV. However, we find that three new background sources (see the Appendix for details) nearby M33 identified by us are not in their background model. We repeated our analysis using the background model excluding these three new background sources and find a similar values of $TS = 35.9$ and $F_{0.1-100\text{GeV}} \sim 2.1 \times 10^{-12} \text{ erg cm}^{-2} \text{ s}^{-1}$ for the best-fit point source model. Thus, we think that the difference between our results and that of Di Mauro et al. (2019) is due to the new background sources.

Our measurement gives a flux of $(1.28 \pm 0.42) \times$

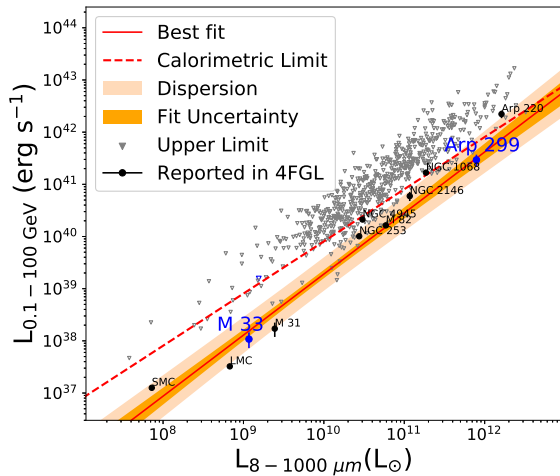


Figure 7. γ -ray luminosities (0.1 – 100 GeV) v.s. total IR luminosities (8 – 1000 μm) for nearby star-forming galaxies. The yellow band represents the empirical correlation $\log(L_{0.1-100 \text{ GeV}}/\text{erg s}^{-1}) = (1.17 \pm 0.07)\log(L_{8-1000 \mu\text{m}}/10^{10}L_{\odot}) + (39.28 \pm 0.08)$ with an intrinsic dispersion normally distributed in the logarithmic space and a standard deviation of $\sigma_D = 0.24$ (Ackermann et al. 2012). The γ -ray luminosities for the galaxies reported in 4FGL are derived from the catalog values (Abdollahi et al. 2020). The IR luminosities are from Sanders et al. (2003). The blue upper downward triangle represents the upper limit for NGC 2403 for the last 5.7-year *Fermi*-LAT data.

$10^{-12} \text{ erg cm}^{-2} \text{ s}^{-1}$ in the energy range 0.1 – 100 GeV, implying a luminosity of $\sim 1.1 \times 10^{38} \text{ erg s}^{-1}$. In Figure 7, we show the position of M33 on the empirical $L_{\gamma} - L_{\text{IR}}$ correlation for local group galaxies and nearby star forming galaxies (Ackermann et al. 2012; Peng et al. 2016). M33 agrees well with this correlation, indicating that the γ -ray emission of M33 may arise from the CR-ISM interaction process.

The TS map of M33 shows that the γ -ray emission locates at the northeast region of the galaxy, where a supergiant H II region, NGC 604, resides. NGC 604 is the second most massive H II region in the Local Group and it has a relatively high star-formation rate. From the H I density distribution map of M33, an over-density of H I gas filament is seen around that region, with a column density of $\sim 30M_{\odot} \text{ pc}^{-2}$ (Engargiola et al. 2003). Such a high-density region provides a thick target for CR-ISM interaction, so the efficiency for the pp collision is expected to be high.

The energy-loss time of protons due to the pp collision t_{loss} can be expressed as $(0.5n\sigma_{pp}c)^{-1}$, where 0.5 is the inelasticity, n is the hydrogen atom number density and σ_{pp} is the inelastic pp collision cross section. Converting the atom number density to gas surface density, $\Sigma_g = m_p n H$, where m_p is the mass of proton and H is the

size of the over-density region, the energy-loss time is

$$t_{\text{loss}} = 6.5 \times 10^6 \left(\frac{H}{200 \text{ pc}} \right) \left(\frac{\sigma_{pp}}{30 \text{ mb}} \right)^{-1} \left(\frac{\Sigma_g}{30 M_{\odot} \text{ pc}^{-2}} \right)^{-1} \text{ yr} \quad (1)$$

where H is the typical width of an H I filament.

CRs are scattered off small-scale magnetic field inhomogeneities randomly and diffuse out of the H I filament. The diffusive escape time is $t_{\text{diff}} = H^2/4D$. Here $D = D_0 (E/E_0)^{\delta}$ is the diffusion coefficient, where D_0 and $E_0 = 3 \text{ GeV}$ are normalization factors, and $\delta = 0 - 1$ depending on the spectrum of interstellar magnetic turbulence. The diffusion time is

$$t_{\text{diff}} = 3 \times 10^5 \left(\frac{H}{200 \text{ pc}} \right)^2 \left(\frac{D_0}{10^{28} \text{ cm}^2 \text{ s}^{-1}} \right)^{-1} \left(\frac{E_p}{3 \text{ GeV}} \right)^{-\delta} \text{ yr}. \quad (2)$$

With $D_0 \sim 10^{27} \text{ cm}^2 \text{ s}^{-1}$, the escape time is comparable to the pp cooling time, and the region may be considered to be a proton calorimeter. Although this value is one order of magnitude smaller than the standard diffusion coefficient in the ISM of our Galaxy, it is not *a priori* impossible. A recent polarisation analysis on Cygnus-X, a massive star-forming region in our Galaxy, has revealed that the turbulence in the region is dominated by the magnetosonic mode (Zhang et al. 2018), which is more effective than the commonly considered Alfvénic mode in CR confinement (Yan & Lazarian 2002). There are also a few giant molecular clouds with mass up to $10^6 M_{\odot}$ spatially associated with NGC 604 (Engargiola et al. 2003), which would enhance the average atom density and subsequently the γ -ray emissivity by a factor of at least a few in that region. In addition, massive stellar winds are probably efficient CR factories (Casse & Paul 1980; Cesarsky & Montmerle 1983; Aharonian et al. 2019), so we expect the CR density around NGC 604 to be higher than the average CR density in the ISM. This may explain why the peak of γ -ray emission locates in the northeast region of M33.

4.2. Arp 299

Arp 299 is one of the most powerful merging galaxy system in the local Universe, at a distance of 44 Mpc (Heckman et al. 1999). The system consists of two galaxies in an advanced merging state, NGC 3690 to the west and IC 694 to the east, plus a small compact galaxy (Hibbard & Yun 1999). The total IR luminosity of both galaxies (NGC 3690+IC 694) are $L_{\text{IR}} = 5.16 \times 10^{11} L_{\odot}$ (Charmandaris et al. 2002), so it belongs to the class of Luminous IR Galaxies (LIRGs). BeppoSAX revealed for the first time the existence of a deeply buried ($N_H = 2.5 \times 10^{24} \text{ cm}^2$) AGN with a unabsorbed luminosity of $L_{0.5-100 \text{ keV}} = 1.9 \times 10^{43} \text{ erg s}^{-1}$ (Della Ceca et al. 2002). Chandra and XMM-Newton observations later confirmed the existence of a strongly absorbed

AGN and located it in the nucleus of NGC 3690, while there is evidence that the second nucleus IC 694 might also host an AGN of lower luminosity (Zezas et al. 2003; Ballo et al. 2004; Iwasawa et al. 2009; Pérez-Torres et al. 2010; Della Ceca et al. 2002; Alonso-Herrero et al. 2013). According to the correlation between the X-ray luminosity ($L_{2-10\text{keV}}$) and the bolometric luminosity (L_{bol}) of X-ray selected AGN (Rosario et al. 2012), we find an intrinsic luminosity of $L_{\text{bol}} \simeq 5 \times 10^{43} \text{erg s}^{-1}$ for the obscured AGN. Even if all the AGN luminosity is reprocessed into the IR band, its contribution is negligible to the measured IR luminosity from the galaxy and hence the latter is related to the star-forming process in Arp 299, as in other star-forming galaxies.

As shown in Fig.5, there is a tentative evidence of flux variability in Arp 299. If this variability is true, it may be due to the contribution from the obscured AGN. Some other merging galaxy systems, such as NGC 3424, also show flux variability in γ -ray emission (Peng et al. 2019). However, different from NGC 3424, Arp 299 lies on the empirical $L_{\gamma} - L_{\text{IR}}$ scaling (see Fig.7). Considering also that the hint of variability is not very significant ($< 3\sigma$), this may indicate that the obscured AGN contributes a subdominant part to the whole γ -ray flux.

4.3. Conclusions

To summarize, our analysis using 11.4 years of *Fermi*-LAT data in new detections of γ -ray emission from M33 and Arp 299. The fluxes of both sources are consistent with the correlation between the γ -ray luminosities and the total IR luminosities for star-forming galaxies, suggesting that γ -ray emissions from the two sources should arise mainly from CRs interacting with the ISM. However, it is found that there is a tentative evidence of variability in the γ -ray flux of Arp 299. The variability can be tested in future with longer observation time. If the variability is true, part of the γ -ray emission should come from the obscured AGN in Arp 299. The morphological analysis of the γ -ray emission from M33 shows that the peak of the TS map is not located at the galaxy center, but coincident with the supergiant H II region NGC 604. This implies that some bright star-forming regions could dominate over the bulk of the galaxy disk in producing γ -ray emission.

A note added: We note that during the final stage of the present work, an independent research paper (Ajello et al. 2020) appears online, which conducted a similar study to that of the present work.

The work is supported by NSFC grants 11625312 and 11851304, and the National Key R & D program of China under the grant 2018YFA0404203.

REFERENCES

- Abdo, A. A., Ackermann, M., Ajello, M., et al. 2010a, ApJL, 709, L152
 —. 2010b, A&A, 523, A46
 —. 2010c, A&A, 523, L2
 —. 2010d, A&A, 512, A7
 Acero, F., Ackermann, M., Ajello, M., et al. 2016, ApJS, 223, 26
 Ackermann, M., Ajello, M., Allafort, A., et al. 2012, ApJ, 755, 164
 Ackermann, M., Albert, A., Atwood, W. B., et al. 2016, A&A, 586, A71
 Ackermann, M., Ajello, M., Albert, A., et al. 2017, ApJ, 836, 208
 Aharonian, F., Yang, R., & de Oña Wilhelmi, E. 2019, Nature Astronomy, 3, 561
 Alonso-Herrero, A., Roche, P. F., Esquej, P., et al. 2013, ApJL, 779, L14
 Atwood, W. B., Abdo, A. A., Ackermann, M., et al. 2009, ApJ, 697, 1071
 Ajello, M., Di Mauro, M., Paliya, V. S. and Garrappa, S., 2020, arXiv:2003.05493
 Ballo, L., Braitto, V., Della Ceca, R., et al. 2004, ApJ, 600, 634
 Casse, M., & Paul, J. A. 1980, ApJ, 237, 236
 Cesarsky, C. J., & Montmerle, T. 1983, SSRv, 36, 173
 Charmandaris, V., Stacey, G. J., & Gull, G. 2002, ApJ, 571, 282
 Della Ceca, R., Ballo, L., Tavecchio, F., et al. 2002, ApJL, 581, L9
 Di Mauro, M., Hou, X., Eckner, C., Zaharijas, G., & Charles, E. 2019, PhRvD, 99, 123027
 Engargiola, G., Plambeck, R. L., Rosolowsky, E., et al. 2003, ApJS, 149, 343
 Griffin, R. D., Dai, X., & Thompson, T. A. 2016, ApJL, 823, L17
 Heckman, T. M., Armus, L., Weaver, K. A., & Wang, J. 1999, ApJ, 517, 130
 Hibbard, J. E., & Yun, M. S. 1999, AJ, 118, 162
 Iwasawa, K., Sanders, D. B., Evans, A. S., et al. 2009, ApJL, 695, L103
 Karwin, C. M., Murgia, S., Campbell, S., & Moskalenko, I. V. 2019, ApJ, 880, 95
 Kennicutt, Robert C., J. 1998, ApJ, 498, 541
 Lacki, B. C., Thompson, T. A., Quataert, E., Loeb, A., & Waxman, E. 2011, ApJ, 734, 107
 Nolan, P. L., Abdo, A. A., Ackermann, M., et al. 2012, ApJS, 199, 31
 Pavlidou, V., & Fields, B. D. 2002, ApJL, 575, L5
 Peng, F.-K., Wang, X.-Y., Liu, R.-Y., Tang, Q.-W., & Wang, J.-F. 2016, ApJL, 821, L20
 Peng, F.-K., Zhang, H.-M., Wang, X.-Y., Wang, J.-F., & Zhi, Q.-J. 2019, ApJ, 884, 91
 Pérez-Torres, M. A., Alberdi, A., Romero-Cañizales, C., & Bondi, M. 2010, A&A, 519, L5
 Persic, M., & Rephaeli, Y. 2010, MNRAS, 403, 1569
 Rosario, D. J., Santini, P., Lutz, D., et al. 2012, A&A, 545, A45
 Sanders, D. B., Mazzarella, J. M., Kim, D. C., Surace, J. A., & Soifer, B. T. 2003, AJ, 126, 1607
 Stecker, F. W. 2007, Astroparticle Physics, 26, 398
 Tang, Q.-W., Wang, X.-Y., & Tam, P.-H. T. 2014, ApJ, 794, 26
 Abdollahi, S., Acero, F., Ackermann, M., et al. 2020, ApJS, 247, 33

Thompson, T. A., Quataert, E., & Waxman, E. 2007, ApJ, 654, 219
 Torres, D. F. 2004, ApJ, 617, 966
 Xi, S. Q., Liu, R. Y., Wang, X. Y. Yang, R. Z., Yuan, Q., Zhang, B, 2020, ApJL, 896, L33 (Paper I)

Yan, H., & Lazarian, A. 2002, PhRvL, 89, 281102
 Yun, M. S., Reddy, N. A., & Condon, J. J. 2001, ApJ, 554, 803
 Zezas, A., Ward, M. J., & Murray, S. S. 2003, ApJL, 594, L31
 Zhang, H., Chepurinov, A., Yan, H., et al. 2018, arXiv e-prints, arXiv:1808.01913

APPENDIX

A. BACKGROUND MODEL FOR M 33 AND ARP 299

As shown in Fig A1, we generated a $6^\circ \times 6^\circ$ TS map based on the background modeling combining the diffuse Galactic emission and the sources listed in 4FGL catalog. For the regions around M 33 and Arp 299, we found three and one obvious excesses outside the galaxy radii, respectively. We locate these four new point sources at the positions of the TS peak and derived their power-law spectral parameter from a broadband spectral fit. The coordinates of four new point sources and their spectral parameters are given in Table A1.

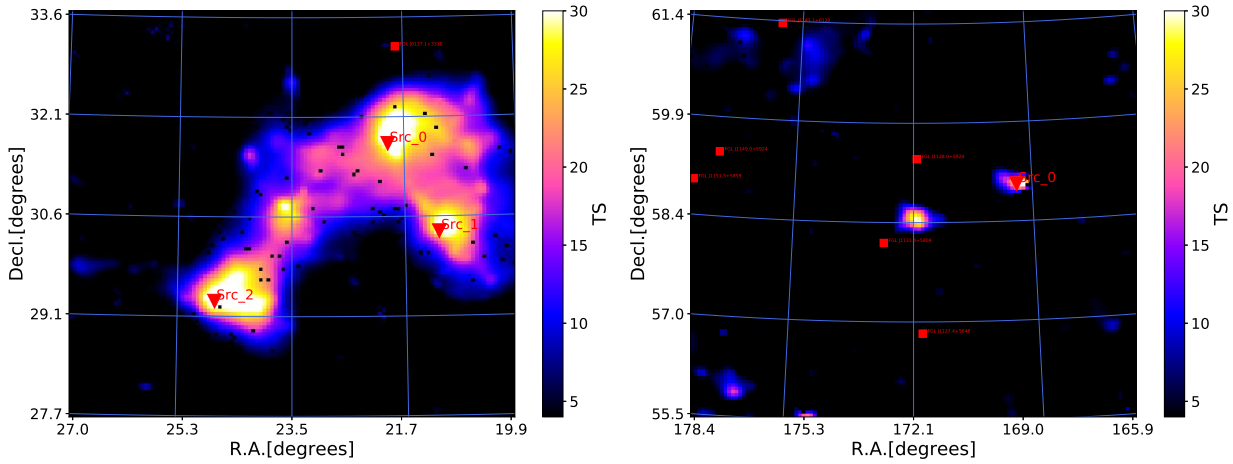


Figure A1. $6^\circ \times 6^\circ$ TS map in the energy band 0.3 – 500 GeV for M 33 (left) and for Arp 299 (right).

Table A1.

Name	TS	$R.A.$ [deg]	Decl. [deg]	N_0 $\times 10^{-14} \text{ cm}^{-2} \text{ s}^{-1} \text{ MeV}^{-1}$	Γ
(1)	(2)	(3)	(4)	(5)	(6)
$6^\circ \times 6^\circ$ region around M33					
Src_0	34.1	21.914	31.711	1.07 ± 0.39	2.75 ± 0.28
Src_1	29.3	21.098	30.439	0.99 ± 0.38	2.77 ± 0.26
Src_2	38.5	24.657	29.36	1.04 ± 0.38	2.87 ± 0.23
$6^\circ \times 6^\circ$ region around Arp 299					
Src_0	32.7	169.308	58.989	0.65 ± 0.21	1.71 ± 0.18

NOTE—The spectrum of each source is modeled as a power law spectrum $dN/dE = N_0(E/E_0)^{-\Gamma}$, where E_0 is fixed to 3 GeV. (1)Source name; (2)TS value; (3) Right ascension J2000 (4) Declination J2000; (5) Power-law spectral normalization N_0 ; (6) Power-law spectral photon index;

To study the impact of different diffuse Galactic emission models, we also created an alternative background model

using the old diffuse Galactic emission template (i.e., `gll_iem_v06.fits`, [Acero et al. 2016](#)). Note that the spectrum of isotropic model is shaped by `iso_P8R3_SOURCE_V2.txt`, which apply to the analysis of Pass 8 events with IRF P8R3_SOURCE_V2 considering the Galactic model `gll_iem_v06.fits`. We generated the TS maps for M33 and for Arp 299 based on this background model, which are shown in Fig. A2. Comparing the new maps to that shown in Fig.1 and Fig.4, we find that the the morphology of the γ -ray excesses from the two galaxies is almost unchanged.

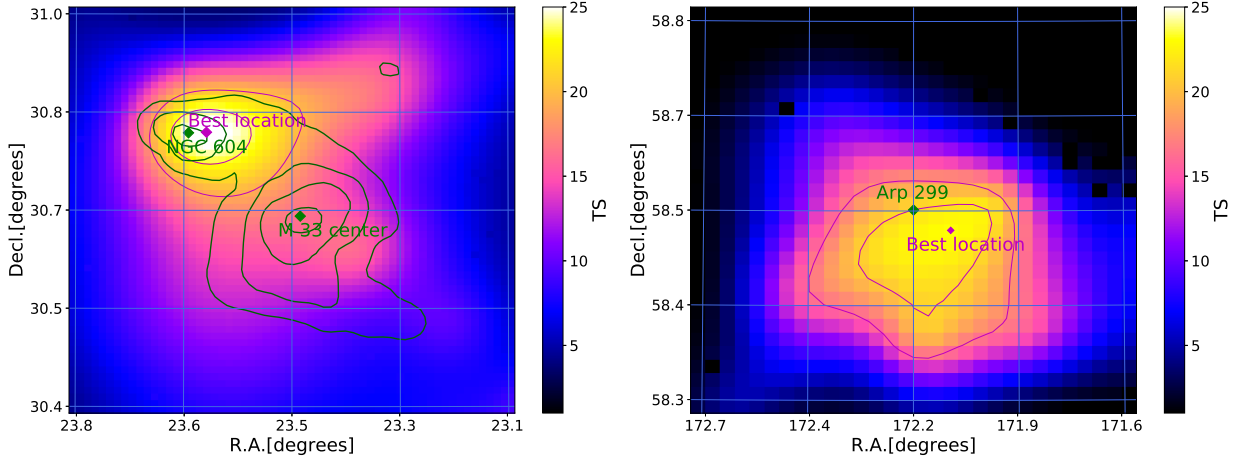


Figure A2. TS map in the energy band 0.3 – 500 GeV for M33 (left) and for Arp 299 (right) with background emission subtracted for the case using the old diffuse Galactic emission template `gll_iem_v06.fits`. The dark green contours correspond to measurements of IRAS at $60\mu\text{m}$.